


Overexpression of neuregulin 1 in GABAergic interneurons results in reversible cortical disinhibition

Yao-Yi Wang^{1,2}, Bing Zhao^{1,2}, Meng-Meng Wu^{1,2}, Xiao-Li Zheng¹, Longnian Lin¹ & Dong-Min Yin¹  [✉]

Cortical disinhibition is a common feature of several neuropsychiatric diseases such as schizophrenia, autism and intellectual disabilities. However, the underlying mechanisms are not fully understood. To mimic increased expression of *Nrg1*, a schizophrenia susceptibility gene in GABAergic interneurons from patients with schizophrenia, we generated *gtoNrg1* mice with overexpression of *Nrg1* in GABAergic interneurons. *gtoNrg1* mice showed cortical disinhibition at the cellular, synaptic, neural network and behavioral levels. We revealed that the intracellular domain of NRG1 interacts with the cytoplasmic loop 1 of Na_v1.1, a sodium channel critical for the excitability of GABAergic interneurons, and inhibits Na_v currents. Intriguingly, activation of GABAergic interneurons or restoring NRG1 expression in adulthood could rescue the hyperactivity and impaired social novelty in *gtoNrg1* mice. These results identify mechanisms underlying cortical disinhibition related to schizophrenia and raise the possibility that restoration of NRG1 signaling and GABAergic function is beneficial in certain neuropsychiatric disorders.

¹Key Laboratory of Brain Functional Genomics, Ministry of Education and Shanghai, School of Life Science, East China Normal University, Shanghai, China.

²These authors contributed equally: Yao-Yi Wang, Bing Zhao, Meng-Meng Wu. ✉email: dmyin@brain.ecnu.edu.cn

Cortical disinhibition is a common feature of several neuropsychiatric diseases such as schizophrenia, autism, and intellectual disabilities¹. However, the underlying molecular and cellular mechanisms are not fully understood. Neuregulin 1 (*Nrg1*) is genetically associated with schizophrenia in diverse populations^{2–4}. The *Nrg1* gene encodes NRG1 protein, a trophic factor implicated in both neurodevelopment and neurotransmission⁵. NRG1 has over 30 splicing isoforms per the different amino acid sequences in the N-terminus⁶. The C-terminal fragment of NRG1 (NRG1-CTF), which is generated by extracellular cleavage, can be further cleaved by γ -secretase to generate the NRG1-intracellular domain (NRG1-ICD)⁶. The amino acid sequences of NRG1-ICD are more conserved among different species than the N-terminus⁷. Most of the single-nucleotide polymorphisms (SNPs) in the *Nrg1* gene that are associated with schizophrenia are localized in intronic, noncoding regions⁶, raising the possibility that they may regulate the expression of the *Nrg1* gene. While some studies showed isoform 1 alpha of *Nrg1* was lower in brains of schizophrenia patients^{8,9}, other studies reported increased *Nrg1* expression or elevated NRG1 signaling in schizophrenia brain^{10–14}. Of note, the increase of *Nrg1* expression in schizophrenia brain did not correlate with antipsychotic treatment^{11,13}, suggesting an association with the disorder instead of medication.

Nrg1 is highly expressed in neurons in the mammalian brain¹⁵. Recent studies based on single-cell RNA sequencing revealed that *Nrg1* was expressed in both inhibitory and excitatory neurons from mouse and human prefrontal cortex (PFC)^{16,17}, a key brain region implicated in schizophrenia^{18,19}. Most postmortem studies analyzed the gene expression in the total homogenate of schizophrenia brain, likely masking cell-type-specific alterations due to cellular heterogeneity²⁰. Two recent studies reported the transcriptome alterations in GABAergic interneurons (mainly were parvalbumin⁺) and pyramidal neurons (PN) from the PFC of schizophrenia patients^{21,22}. Here, we analyzed the cell-type-specific *Nrg1* expression in the GEO database: GSE93577 and GSE93987^{21,22}. We found that *Nrg1* expression was increased in GABAergic interneurons but not in PN from the PFC of schizophrenia patients, compared with age- and sex-matched healthy controls.

To mimic increased *Nrg1* expression in GABAergic interneurons from schizophrenia patients, we generated *gtoNrg1* mice in which *Nrg1* overexpression specifically occurred in GABAergic interneurons and could be turned off by doxycycline (Dox). Intriguingly, *gtoNrg1* mice showed cortical disinhibition at the cellular, synaptic, and neural network levels. The mechanistic study suggested that NRG1-ICD could interact with Na_v1.1, a sodium channel critical for the excitability of GABAergic interneurons and inhibit the Na_v currents. We further demonstrated that cortical disinhibition led to behavioral deficits in *gtoNrg1* mice. Lastly, both cortical disinhibition and behavioral deficits in *gtoNrg1* mice disappeared when NRG1 expression returned to normal in adulthood. Together, our results demonstrate mechanisms underlying cortical disinhibition related to schizophrenia and shed light on the pathophysiology of neuropsychiatric disorders.

Results

Generation of *gtoNrg1* mice to mimic increased *Nrg1* expression in GABAergic interneurons from schizophrenia patients.

To address the cell-type-specific alteration of *Nrg1* gene expression in the postmortem PFC of schizophrenia patients, we analyzed the GEO database GSE93577²¹ and GSE93987²². The database GSE93577 was composed of gene expression data in GABAergic interneurons from 36 schizophrenia patients and 36

matched healthy controls (Supplementary Table 1). The database GSE93987 included the gene expression data in layer 3 PN from the same PFC samples as database GSE93577 (Supplementary Table 1). Type I *Nrg1* mRNA levels were significantly increased in GABAergic interneurons from schizophrenia PFC, compared with age- and sex-matched controls (Fig. 1a). By contrast, *Nrg1* mRNA levels were not significantly altered in PN from schizophrenia PFC, compared to age- and sex-matched controls (Fig. 1b). The increased type I *Nrg1* expression in GABAergic interneurons from schizophrenia PFC seems not to be due to the antipsychotic treatment because type I *Nrg1* mRNA levels were similar between drug-naïve and drug-treated schizophrenia patients (Supplementary Fig. 1a). There is no sex difference for type I *Nrg1* expression in the schizophrenia PFC (Supplementary Fig. 1b). Type IV *Nrg1* expression was not significantly increased in GABAergic interneurons from schizophrenia PFC (Supplementary Fig. 1c), suggesting a specificity for an increase of type I *Nrg1* expression in GABAergic interneurons. Neuregulin 3 (*Nrg3*) is another schizophrenia risk factor among the neuregulin gene family^{23–25}. By contrast, the mRNA levels of *Nrg3* were reduced in GABAergic interneurons from schizophrenia PFC, compared with age- and sex-matched controls (Supplementary Fig. 1d). Together, these results suggest that type I *Nrg1* expression is increased in GABAergic interneurons from the postmortem PFC of schizophrenia patients.

To mimic the increased type I *Nrg1* expression in GABAergic interneurons from schizophrenia patients, we aim to generate *Nrg1* transgenic mice that overexpress type I *Nrg1* specifically in GABAergic interneurons. Toward this goal, TRE-*Nrg1* mice (Fig. 1c)²⁶ were crossed with *Gad67*-tTA mice which express tTA specifically in GABAergic interneurons²⁷ (Supplementary Fig. 2). Resulting *Gad67*-tTA; TRE-*Nrg1* mice (*gtoNrg1* for *Gad67* promoter-driven *tet-off Nrg1*) produced HA-NRG1 in GABAergic interneurons in the absence of Dox (Fig. 1d). We used *Gad67*-tTA mice as controls in the following experiments (see also the methods). As shown in Fig. 1e, the mRNA of *Nrg1* was increased in several brain regions including olfactory bulb (OB), striatum (STR), and prefrontal cortex (PFC) in *gtoNrg1* mice, compared with controls. The increase was due to the expression of the transgene, which was detectable by the expression of the HA tag (Fig. 1f). In agreement, the protein levels of NRG1 (including the full length and ICD) were increased by 50–100% in the PFC of *gtoNrg1* mice (Fig. 1g, h). To demonstrate the *Nrg1* transgene is specifically expressed in GABAergic interneurons in the PFC, we performed single-cell RT-PCR. As shown in Supplementary Fig. 1e, the *Nrg1* transgene indicated by the expression of HA tag was expressed in GABAergic interneurons but not in PN. Lastly, overexpression of *Nrg1* could be switched off by feeding the mice with Dox-containing water (Fig. 1e–h). Together, the results indicate that *gtoNrg1* mice express higher levels of *Nrg1* specifically in GABAergic interneurons, and the overexpression could be turned off efficiently by Dox.

Behavioral deficits in *gtoNrg1* mice. *gtoNrg1* mice showed similar body weight with control littermates (Supplementary Fig. 3a), indicating no growth retardation. However, they were hyperactive in the open-field test (Fig. 2a), a phenotype related to abnormalities of brain dopamine levels in schizophrenia patients. By contrast, the staying time in the margin and center of the open field was similar between control and *gtoNrg1* mice (Supplementary Fig. 3b), indicating no anxiety-like phenotype. Prepulse inhibition (PPI) is a common test of sensorimotor gating that is often impaired in schizophrenia patients²⁸. *gtoNrg1* mice had a normal response to 75–85 dB background noise (Supplementary Fig. 3c–e). The prepulse itself has significant effects on PPI in both control and

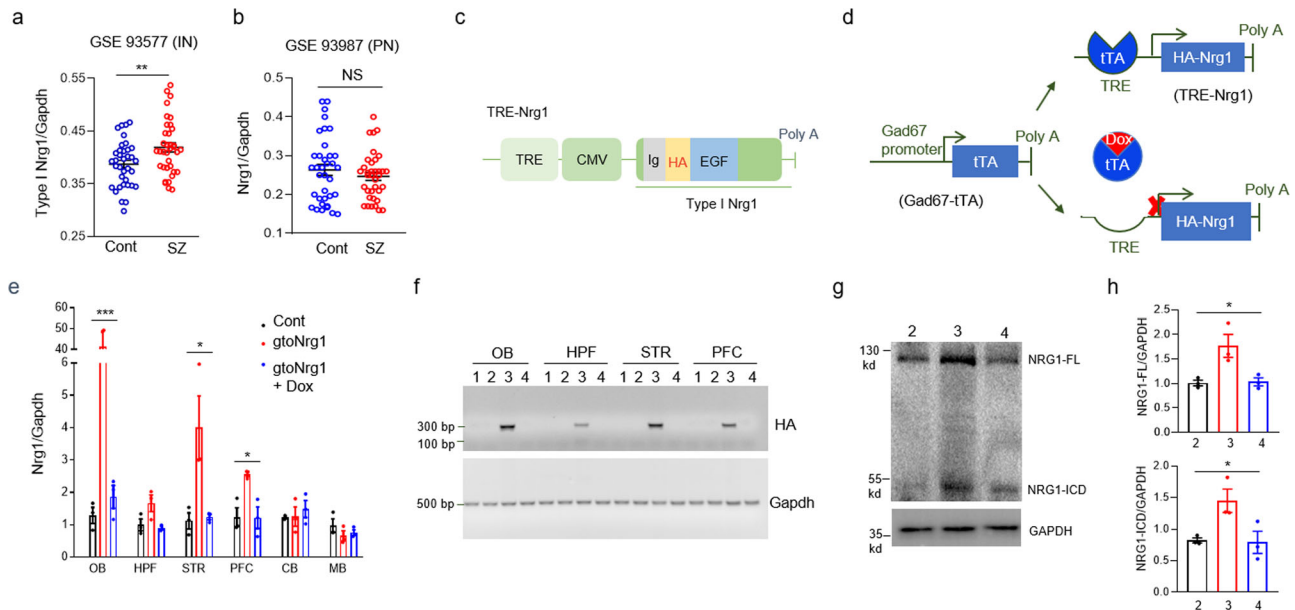


Fig. 1 Generation of *gtoNrg1* mice to mimic increased *Nrg1* expression in GABAergic interneurons from schizophrenia patients. **a** Increased type I *Nrg1* mRNA levels in GABAergic interneurons from schizophrenia PFC, compared with age- and sex-matched controls. $**P = 0.0064$, two-sided *t* test, $n = 36$ for each group. Data are presented as mean values \pm SEM. **b** Similar *Nrg1* expression in pyramidal neurons from layer 3 PFC between control and schizophrenia patients. NS, not significant, two-sided *t* test, $n = 36$ for each group. Data are presented as mean values \pm SEM. Cont control, SZ schizophrenia, IN GABAergic interneurons, PN pyramidal neurons. The levels of *Nrg1* mRNA were normalized to that of *Gapdh*. **c** Full-length *Nrg1* type I β 1a was cloned in pMM400 between the promoter complex of TRE and CMV (cytomegalovirus minimal promoter) and SV40 polyadenylation (Poly A) signal. An HA tag was inserted between the Ig and EGF domain of NRG1. **d** The principle of the tet-off system. HA-*Nrg1* is expressed in *Gad67-tTA*; TRE-*Nrg1* (*gtoNrg1*) mice. The expression of HA-*Nrg1* can be switched off by Dox. **e** Increased *Nrg1* mRNA levels in different brain regions of *gtoNrg1* mice. The *Nrg1* mRNA levels return to normal after Dox treatment for 5 days. $*P$ (PFC) = 0.0157, $*P$ (STR) = 0.0223, $***P = 0.001$, one-way-ANOVA, $n = 3$ mice for each group. Data are presented as mean values \pm SEM. OB olfactory bulb, HPF hippocampus formation, STR striatum, PFC prefrontal cortex, CB cerebellum, MB midbrain. **f** Expression of HA tag in *gtoNrg1* mice. Three independent experiments were repeated to get similar results. The homogenate from different brain regions was subjected to RT-PCR assay for HA and *Gapdh*. (1) TRE-*Nrg1*; (2) *Gad67-tTA*; (3) *gtoNrg1*; (4) *gtoNrg1* + Dox. **g** Increased NRG1 protein levels (including the full length and ICD) in the PFC of *gtoNrg1* mice. The homogenate of PFC from different mice was subjected to western blot and probed with anti-NRG1 and anti-GAPDH Abs. (2) control; (3) *gtoNrg1*; (4) *gtoNrg1* + Dox. **h** Quantification of the expression of full-length NRG1 (top) and NRG1-ICD (bottom) in panel **g**. $*P = 0.0178$ for NRG1-FL, $*P = 0.034$ for NRG1-ICD, one-way-ANOVA, $n = 3$ mice for each group, data were normalized to controls. Data are presented as mean values \pm SEM.

gtoNrg1 mice (Supplementary Fig. 3f, g). However, the startle response to 120 dB and PPI were compromised in *gtoNrg1* mice compared with controls (Fig. 2b, c). In the prepulse + pulse trails, both genotypes reduce their startle response with increasing intensity of the prepulse (Fig. 2d). There is a minor but significant difference in the extent to which the prepulse gates the startle response to the pulse between two genotypes (interaction (prepulse \times genotype) $F(2, 84) = 3.136$, $P = 0.0486$, two-way ANOVA) (Fig. 2d). Together, these results suggest that overexpression of *Nrg1* in GABAergic interneurons impairs startle response and has minor effects on sensorimotor gating.

Impaired social behavior is a negative symptom of schizophrenia²⁹. *gtoNrg1* mice could distinguish the stimulus mouse and the objective in the three-chamber test, similar to controls (Supplementary Fig. 3h, i), suggesting normal social interaction. However, *gtoNrg1* mice spent lesser time in the chamber with novel mice (S2) but stayed longer in the chamber with familiar mice (S1), compared with controls (Fig. 2e–g), indicating impaired social novelty. The reduced social novelty of *gtoNrg1* mice may not result from the deficient olfaction because *gtoNrg1* mice showed better olfaction during finding the buried food compared with controls (Supplementary Fig. 3j). We also studied nesting behavior in control and *gtoNrg1* mice to assess their ability to establish an organized behavior. Compared with controls, *gtoNrg1* mice were unable to build an identifiable nest within 12 h (Fig. 2h, i).

We next determined whether overexpressing *Nrg1* in GABAergic interneurons affected spatial recognition memory in Y maze. To exclude the potential influence of hyperactivity in the Y-maze test, we analyzed the time exploring the start, old and new arms (Fig. 2j, k). Although there was a preference for the new arm in both control and *gtoNrg1* mice (Fig. 2l, m), the percentage of time exploring the new arm was significantly reduced in *gtoNrg1* mice compared with controls (Fig. 2n). These results suggest that *gtoNrg1* mice have impaired spatial recognition memory.

Hypersynchrony of neural network in the PFC of *gtoNrg1* mice. Given the evidence of PFC-mediated behavioral deficit such as an impaired social novelty in *gtoNrg1* mice, we next studied how the neural network of PFC was altered in *gtoNrg1* mice. Here, we focus on layers 2–3 of PFC because the layer 3 circuitry in PFC is significantly altered in schizophrenia patients³⁰. To this end, we carried out local field potential (LFP) recordings in the PFC of freely behavioral control and *gtoNrg1* mice. We acutely implanted 32-channel tetrodes in the layer 2–3 of PrL (prelimbic cortex, a major region of PFC, Fig. 3a), and after 2 weeks of recovery, the LFP was recorded. We analyzed epochs of activity in which the speed of movement was above 3 cm/s to reduce variability in LFP recordings, and we verified that the mean speed of the epochs analyzed was similar for both genotypes. Analysis of spontaneous LFPs in layers 2–3 of PrL revealed a significant

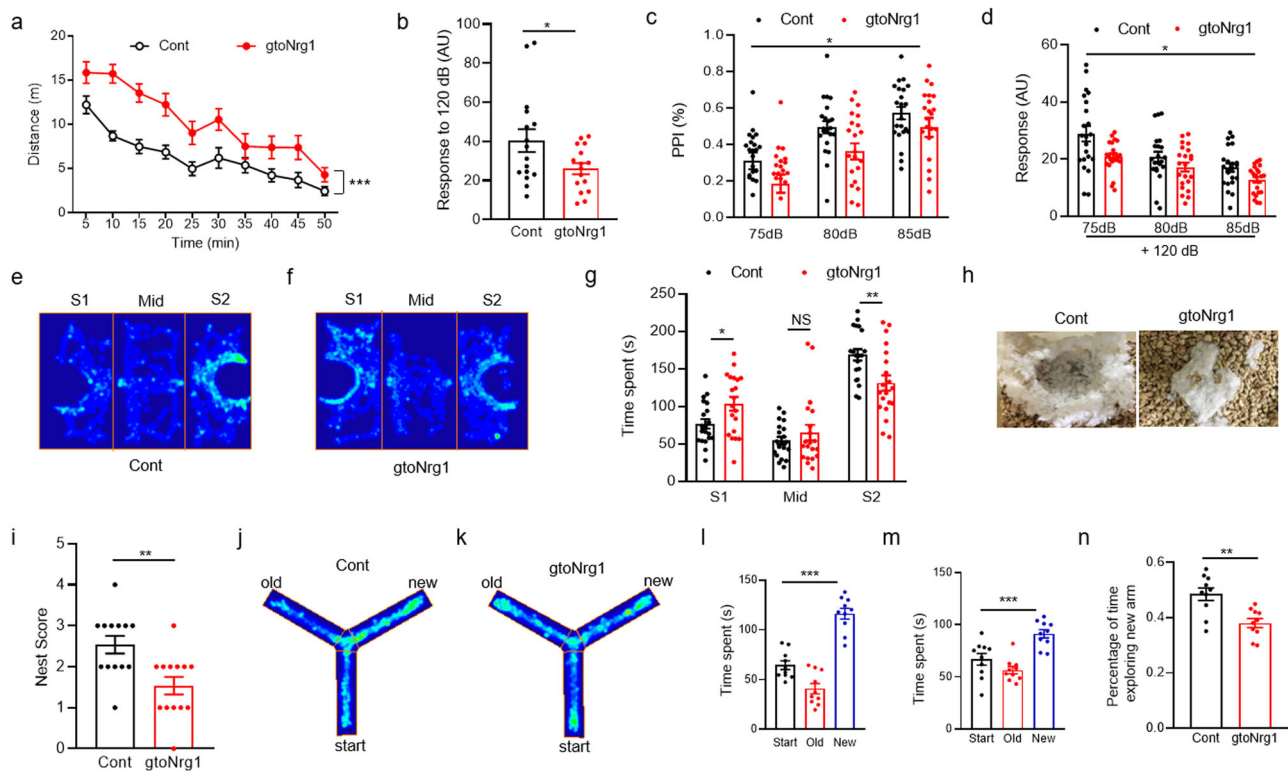


Fig. 2 Behavioral deficits in *gtoNrg1* mice. **a** Travel distance in open field was increased in *gtoNrg1* mice compared with controls. ***Genotype $F(1, 28) = 15.74$, $P = 0.0005$, two-way ANOVA, $n = 15$ for each group. Data are presented as mean values \pm SEM. **b** Reduced startle response to 120 dB noise in *gtoNrg1* mice compared with controls. * $P = 0.0356$, two-sided t test, $n = 16$ for each group. Data are presented as mean values \pm SEM. **c** Impaired PPI in *gtoNrg1* mice compared with controls. *Genotype $F(1, 42) = 4.9$, $P = 0.0324$, two-way ANOVA, $n = 22$ for each group. Data are presented as mean values \pm SEM. **d** Reduced reflex amplitudes on prepulse + pulse trials in *gtoNrg1* mice compared with controls. *Genotype $F(1, 42) = 6.11$, $P = 0.0176$, ***Prepulse $F(1.709, 71.78) = 53.69$, $P < 0.0001$, *Interaction (prepulse \times genotype) $F(2, 84) = 3.136$, $P = 0.0486$, two-way ANOVA, $n = 22$ for each group. Data are presented as mean values \pm SEM. **e, f** Occupancy plot of the heads from control (**e**) and *gtoNrg1* (**f**) mice in the three-chamber test. S1, familiar mouse; S2, novel mouse. **g** Reduced social novelty in *gtoNrg1* mice compared with controls. Time spent in each chamber was quantified. NS not significant, * $P = 0.02$, ** $P = 0.0056$, two-sided t test, $n = 20$ for each group. Data are presented as mean values \pm SEM. **h, i** Impaired nest building in *gtoNrg1* mice compared with controls. **h** Representative images for a nest built after 12 h. **i** Quantification of nest score. ** $P = 0.0031$, two-sided t test, $n = 13$ for each group. Data are presented as mean values \pm SEM. **j, k** Occupancy plot of the heads from control (**j**) and *gtoNrg1* (**k**) mice in Y maze. **l, m** Preference for the new arm in control (**l**) and *gtoNrg1* (**m**) mice. The time exploring the start, old, and new arms was quantified. *** $P < 0.001$, one-way ANOVA, $n = 10$ for each group. Data are presented as mean values \pm SEM. **n** Impaired spatial recognition memory in *gtoNrg1* mice compared with controls. The percentage of time exploring a new arm in the Y maze was quantified. ** $P = 0.0016$, two-sided t test, $n = 10$ for each group. Data are presented as mean values \pm SEM.

increase of activity in *gtoNrg1* mice, compared with controls (Fig. 3b, c). Next, we analyzed the relative power of oscillations in control and *gtoNrg1* mice. We observed a significant increase in the relative power of delta (0.5–3 Hz), theta (4–12 Hz), alpha (13–15 Hz), and beta (16–30 Hz) oscillations in *gtoNrg1* mice, compared with controls (Fig. 3d–k). The relative power of gamma (30–90 Hz) and high-frequency oscillation (HFO) (>100 Hz) were not significantly altered in the PFC of *gtoNrg1* mice, compared to controls (Fig. 3f, l–n). These results suggest that overexpression of *Nrg1* in GABAergic interneurons led to hypersynchrony of the neural network in the PFC.

Elevated E/I balance in the PFC of *gtoNrg1* mice. The hypersynchrony of neural networks in *gtoNrg1* mice may reflect an alteration in E/I balance. Next, we sought to determine whether the E/I ratio was changed in the PFC of *gtoNrg1* mice. Toward this aim, we performed a whole-cell patch clamp to record the spontaneous excitatory and inhibitory postsynaptic currents (sEPSC and sIPSC) from layers 2 to 3 PN in PrL (Fig. 4a). As shown in Fig. 4b–f, the frequency but not the amplitude of sEPSC was significantly increased in *gtoNrg1* mice, compared with

controls. By contrast, the frequency but not amplitude of sIPSC was reduced in *gtoNrg1* mice, compared with controls (Fig. 4g–k). In support of these results was the observation that the E/I ratio was elevated in the *gtoNrg1* PFC, compared with controls (Fig. 4l). The reduced sIPSC frequency in *gtoNrg1* mice (Fig. 5g, h, j) might be due to the decreased GABAergic synapse number or the impaired ability of GABA release. However, these possibilities could be small because the miniature IPSC (mIPSC) (Supplementary Fig. 4a–c) and paired-pulse ratio (PPR) of evoked IPSC (eIPSC) (Supplementary Fig. 4d, e) from layers 2 to 3 PN in the PrL were similar between control and *gtoNrg1* mice.

We next investigate whether the reduced sIPSC frequency in *gtoNrg1* mice results from the lower excitability of GABAergic interneurons. To visualize the GABAergic interneurons, we crossed *Gad67-tTA* and *gtoNrg1* mice with TRE-Histone 2B (H2B)-GFP mice³¹ to get *gtoGfp* and *gtoNrg1; Gfp* mice, respectively. These mice express H2B-GFP specifically in GABAergic interneurons (Supplementary Fig. 2) and were subject to whole-cell recording in PFC slices (Fig. 4m). The *gtoNrg1; Gfp* mice showed normal laminar structure and densities of GABAergic interneurons in PFC (Supplementary Fig. 5). The

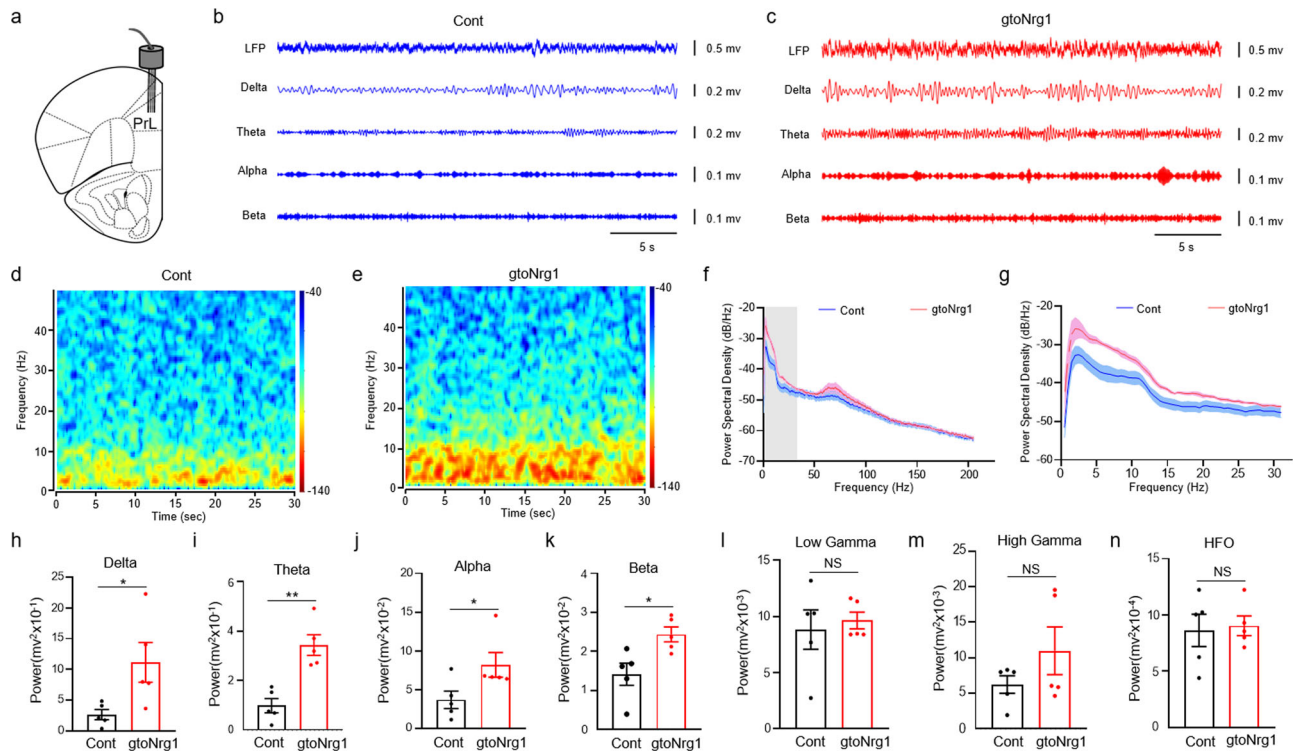


Fig. 3 Increased delta, theta, alpha, and beta oscillation in the PFC of freely behavioral *gtoNrg1* mice. **a** Diagram to show the LFP recording in layers 2–3 of PrL. **b, c** Spontaneous LFP and filtered delta, theta, alpha, and beta component of the signal from control (**b**) and *gtoNrg1* mice (**c**). **d, e** Power spectrogram of LFP from control (**d**) and *gtoNrg1* mice (**e**). **f** Power spectral density of LFP from 0.5 to 200 Hz in control and *gtoNrg1* mice. $n = 5$ for each group. Data are presented as mean values \pm SEM. **g** Power spectral density of LFP from 0.5 to 30 Hz in control and *gtoNrg1* mice. $n = 5$ for each group. Data are presented as mean values \pm SEM. **h–n** LFP band-power in the delta (0.5–3 Hz) (**h**), theta (4–12 Hz) (**i**), alpha (13–15 Hz) (**j**), beta (16–30 Hz) (**k**), low gamma (30–50 Hz) (**l**), high gamma (55–90 Hz) (**m**), and high-frequency oscillation (HFO, 100–300 Hz) (**n**). NS, not significant, $*P = 0.0345$ for panel **h**, $**P = 0.0013$ for panel **i**, $*P = 0.0498$ for panel **j**, $*P = 0.0174$ for panel **k**, two-sided t test, $n = 5$ for each group. Data are presented as mean values \pm SEM.

firing rate varied between fast-spiking (FS) and non-FS-GABAergic interneurons. Here, we focus on FS-GABAergic interneurons whose function is critical for neuronal synchronization and is heavily diminished in the PFC from schizophrenia patients³². Intriguingly, the FS-GABAergic interneurons showed a downward shift of input–output (I/O) curves of action potential (AP) in *gtoNrg1*; *Gfp* mice, compared with *gtoGfp* mice (Fig. 4n, o), suggesting reduced excitability of FS-GABAergic interneurons in *gtoNrg1*; *Gfp* mice.

To further study whether the disinhibition of FS-GABAergic interneurons would increase the firing rate of PN, we recorded AP from PN in control and *gtoNrg1* PFC slices (Fig. 4p). As shown in Fig. 4q, r, the PN firing was significantly increased in *gtoNrg1* mice compared with controls. However, the electrophysiological characteristics of PN were not altered in *gtoNrg1* mice (Supplementary Table 2), indicating that the increased firing rate of PN was secondary to GABAergic hypofunction. Taken together, these results demonstrate that overexpressing NRG1 in GABAergic interneurons causes GABAergic deficit and increases the E/I ratio.

Reduced Na_v currents in GABAergic interneurons from *gtoNrg1* mice. The reduced excitability of FS-GABAergic interneurons in *gtoNrg1*; *Gfp* mice was reflected by the higher rheobase, the minimal currents to produce an AP (Fig. 5a). The intrinsic excitability of GABAergic interneurons was determined by several factors, such as rest membrane potential (RMP), action potential threshold (APT), and afterhyperpolarization (AHP). To isolate intrinsic AP waveform

characteristics, we evoked a single AP with a brief suprathreshold current injection. As shown in representative traces and corresponding dV/dt phase plots (Fig. 5b), the FS-GABAergic interneurons from *gtoNrg1*; *Gfp* mice had a depolarized APT, compared with *gtoGfp* mice. In accord, APT was significantly increased in FS-GABAergic interneurons from *gtoNrg1*; *Gfp* mice, compared with *gtoGfp* mice (Fig. 5a), indicating a role of depolarized APT in reduced excitability. Voltage-gated sodium (Na_v) channels play critical roles in AP generation and threshold³³. To address whether *Nrg1* overexpression affected Na_v currents, we performed voltage-clamp recording on GABAergic interneurons from *gtoGfp* and *gtoNrg1*; *Gfp* PFC slices (Fig. 5c). The I/V curves of Na_v channel activation in GABAergic interneurons showed a downward shift in *gtoNrg1*; *Gfp* mice, compared with *gtoGfp* mice (Fig. 5d). In accord, the maximal Na^+ current density was significantly decreased in GABAergic interneurons from *gtoNrg1*; *Gfp* mice, compared with *gtoGfp* mice (*gtoNrg1*; *Gfp*: -185.85 ± 13.97 pA/pF, $n = 13$, *GtoGfp*: -267.63 ± 22.41 pA/pF, $n = 17$, $P = 0.0077$, t test). By contrast, membrane depolarizations required for half-maximal activation of Na_v channels in GABAergic interneurons were similar between *gtoNrg1*; *Gfp* and *gtoGfp* mice ($V_{1/2} = -29.86 \pm 0.76$ mV for *gtoNrg1*; *Gfp*, $n = 13$, $V_{1/2} = -29.32 \pm 0.56$ mV for *gtoGfp*, $n = 17$, $P = 0.9257$, t test) (Fig. 5e). Together, these results indicated that *Nrg1* overexpression attenuated the peak Na^+ current density but without affecting the voltage dependence of Na_v channel activation.

The reduced Na^+ current density from *gtoNrg1*; *Gfp* mice could be due to the lower protein levels or the impaired function

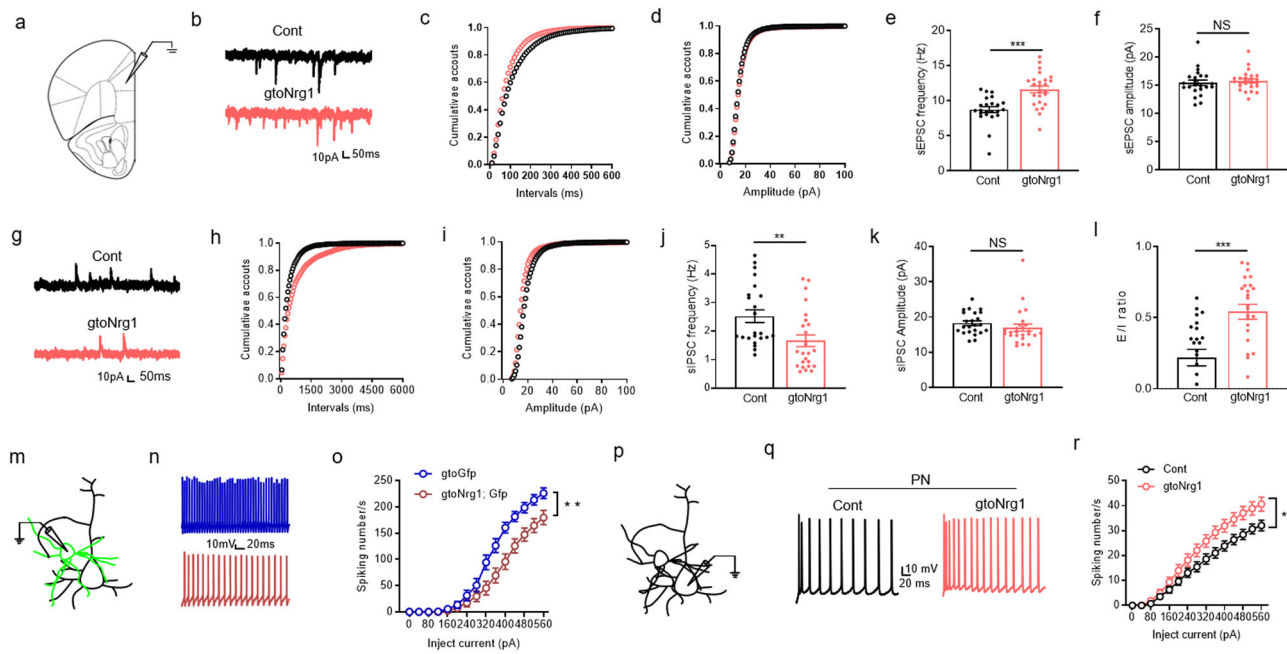


Fig. 4 Elevated E/I balance in the PFC of *gtoNrg1* mice. **a** Diagram to show the whole-cell recording in layers 2–3 of PrL. **b** Representative traces of sEPSC from control and *gtoNrg1* mice. **c, d** Cumulative plots of sEPSC frequency (**c**) and amplitude (**d**). **e** Increased sEPSC frequency in *gtoNrg1* mice. $***P < 0.0001$, two-sided *t* test, $n = 23$ cells from four control mice, $n = 25$ cells from four *gtoNrg1* mice. Data are presented as mean values \pm SEM. **f** Similar sEPSC amplitude between control and *gtoNrg1* mice. NS not significant, two-sided *t* test, $n = 23$ cells from four control mice, $n = 25$ cells from four *gtoNrg1* mice. Data are presented as mean values \pm SEM. **g** Representative traces of sIPSC from control and *gtoNrg1* mice. **h, i** Cumulative plots of sIPSC frequency (**h**) and amplitude (**i**). **j** Reduced sIPSC frequency in *gtoNrg1* mice. $**P = 0.0068$, two-sided *t* test, $n = 23$ cells from four control mice, $n = 25$ cells from four *gtoNrg1* mice. Data are presented as mean values \pm SEM. **k** Similar sIPSC amplitude between control and *gtoNrg1* mice. NS not significant, two-sided *t* test, $n = 23$ cells from four control mice, $n = 25$ cells from four *gtoNrg1* mice. Data are presented as mean values \pm SEM. **l** Elevated E/I ratio in *gtoNrg1* mice. $***P = 0.0002$, two-sided *t* test, $n = 23$ cells from four control mice, $n = 25$ cells from four *gtoNrg1* mice. Data are presented as mean values \pm SEM. **m** Diagram to show the recording of GABAergic interneurons expressing EGFP. **n** Representative action potentials of FS-GABAergic interneurons. **o** Reduced excitability of FS-GABAergic interneurons in *gtoNrg1*; Gfp mice, compared with *gtoGfp* mice. Shown are the I/O curves of action potentials from FS-GABAergic interneurons. $**$ Genotype $F(1, 36) = 8.813$, $P = 0.0053$, two-way ANOVA, $n = 17$ cells from five *gtoGfp* mice, $n = 21$ cells from four *gtoNrg1*; Gfp mice. Data are presented as mean values \pm SEM. **p** Diagram to show the recording of PN. **q** Representative action potentials of PN. **r** Increased excitability of PN in *gtoNrg1* mice compared with controls. Shown are the I/O curves of action potentials from PN. $*$ Genotype $F(1, 50) = 5.041$, $P = 0.0292$, two-way ANOVA, $n = 27$ cells from five control mice, $n = 25$ cells from four *gtoNrg1* mice. Data are presented as mean values \pm SEM.

of Na_v channels caused by *Nrg1* overexpression. There are four isoforms of Na_v channels (Na_v 1.1, Na_v 1.2, Na_v 1.3, and Na_v 1.6) which are primarily expressed in the central nervous system³³. The α -subunits of Na_v are necessary for forming a functional ion-selective channel. The α -subunits of Na_v 1.1, Na_v 1.2, Na_v 1.3, and Na_v 1.6 are encoded by the gene *Scn1a*, *Scn2a1*, *Scn3a*, and *Scn8a*. We analyzed the transcription levels of the four *Scn* genes in the seven major neuronal clusters from the mouse frontal cortex accessible through an online database DropViz (<https://dropviz.org>)¹⁶ (Supplementary Fig. 6). *Scn1a*, *Scn2a1*, and *Scn8a* are the three major *Scn* isoforms expressed in GABAergic interneurons (Fig. 5f). The *SCN1A*, *SCN2A1*, and *SCN8A* proteins are similar in structure and have 74% similarity in the overall amino acid sequences³³. The expression levels of *Scn1a* was higher in GABAergic interneurons, but lower in PN compared with *Scn2a1* and *Scn8a* (Fig. 5f, g). These results are consistent with the previous finding that *Scn1a* is highly expressed in PV-positive GABAergic interneurons and is critical for their excitability³⁴. Due to these reasons, we focused on *Scn1a* in the following study. Neither the mRNA nor the protein levels of *Scn1a* were reduced in *gtoNrg1* PFC, compared to controls (Supplementary Fig. 7a, b). The *SCN1A* protein levels in the membrane fraction were also similar between control and *gtoNrg1* PFC (Supplementary

Fig. 7c). Together with the data in Fig. 5a–e, these results suggest that overexpression of *Nrg1* impairs the function of Na_v channels rather than inhibits the gene expression or membrane trafficking of *SCN1A*.

Inhibition of Na_v currents in GABAergic interneurons by NRG1-ICD. ErbB4 is the main receptor of NRG1 in GABAergic interneurons^{35–37}. We next determine whether the protein levels or activity of ErbB4 were changed in *gtoNrg1* mice. To this end, the homogenate of PFC from control and *gtoNrg1* mice were subjected to western blots and probed with antibodies against ErbB4 and p-ErbB4. As shown in Supplementary Fig. 8, the protein levels of ErbB4 and p-ErbB4 were not altered in *gtoNrg1* PFC, compared to controls. These results suggest that ErbB4 was not activated in the PFC of *gtoNrg1* mice. To study whether the NRG1 EGF domain could reduce Na_v currents in GABAergic interneurons, we incubated the PFC slices with 5 nM NRG1 EGF domain or BSA (as a control). NRG1 EGF domain could promote evoked GABA release (Supplementary Fig. 9a, b), which is consistent with our previous findings^{38–40}. However, the NRG1 EGF domain did not alter the Na_v currents in GABAergic interneurons (Supplementary Fig. 9c, d).

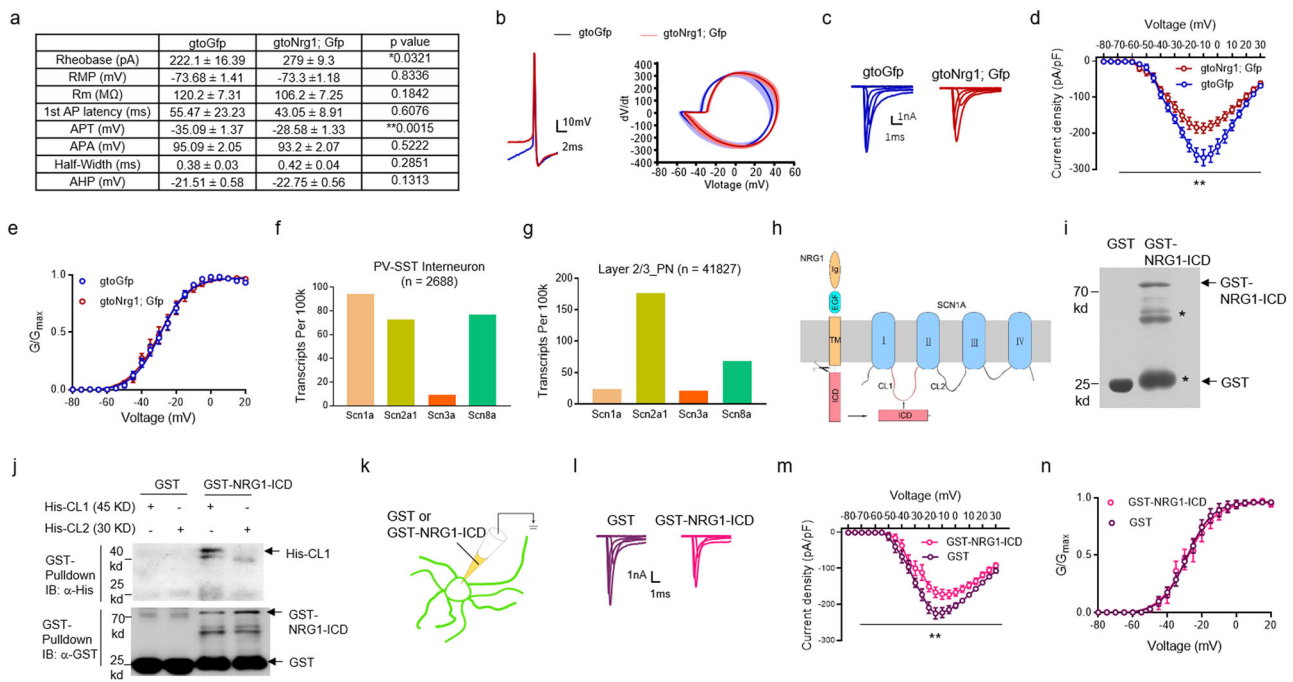


Fig. 5 Inhibition of Na_v currents in GABAergic interneurons by NRG1-ICD. **a** Increased rheobase and depolarized action potential threshold (APT) in the FS-GABAergic interneurons of *gtoNrg1; Gfp* mice, compared with *gtoGfp* mice. * $P = 0.0321$, ** $P = 0.0015$, two-sided t test, $n = 17$ cells from five *gtoGfp* mice, $n = 21$ cells from four *gtoNrg1; Gfp* mice. **b** Representative traces of a single AP evoked from a suprathreshold current injection (left) and corresponding phase plots (dV/dt vs voltage) (right) recorded in FS-GABAergic interneurons from *gtoGfp* and *gtoNrg1; Gfp* mice. **c** Reduced Na^+ current density in GABAergic interneurons from *gtoNrg1; Gfp* PFC. Representative current traces of Na_v channels in GABAergic interneurons from *gtoNrg1; Gfp* and *gtoGfp* mice. Currents were elicited by step depolarizations from -80 to $+30$ mV in 5 mV increments from a holding potential of -80 mV. The tracts shown are for depolarizations from -80 to $+20$ mV. **d** I/V curves of Na_v channel activation in GABAergic interneurons from *gtoNrg1; Gfp* and *gtoGfp* mice. **Genotype $F(1, 28) = 8.264$, $P = 0.0076$, two-way ANOVA, $n = 13$ cells from three *gtoNrg1; Gfp* mice, $n = 17$ cells from four *gtoGfp* mice. Data are presented as mean values \pm SEM. **e** Similar voltage-dependent activation curves of Na_v channels in GABAergic interneurons from *gtoNrg1; Gfp* and *gtoGfp* mice. Genotype $F(1, 28) = 0.023$, $P = 0.879$, two-way ANOVA, $n = 13$ cells from three *gtoNrg1; Gfp* mice, $n = 17$ cells from four *gtoGfp* mice. Data are presented as mean values \pm SEM. **f** Transcriptional levels of *Scn1a* is higher than *Scn2a1*, *Scn3a*, and *Scn8a* in PV and SST-positive GABAergic interneurons ($n = 2688$ cells). Shown are transcripts of *Scn* genes per 100 k total transcripts from single-cell RNA sequencing. **g** Transcriptional levels of *Scn1a* were lower than *Scn2a1* and *Scn8a* in layer 2/3 PN ($n = 41827$ cells). Shown are transcripts of *Scn* genes per 100 k total transcripts from single-cell RNA sequencing. **h** Diagram showing the structure of SCN1A. The SCN1A protein was composed of four transmembrane domains (I–IV) and two major cytoplasmic loops (CL1 and CL2). The NRG1-ICD could interact with the CL1 of SCN1A. **i** Coomassie blue staining of 30 μg GST and GST-NRG1-ICD proteins. Asterisks indicated degradation product of GST-NRG1-ICD proteins. Four independent experiments were repeated to get similar results. **j** Interaction of NRG1-ICD with His-CL1. The recombinant GST-NRG1-ICD and His-CL1, or His-CL2 proteins were used for GST pull-down experiments. Four independent experiments were repeated to get similar results. **k** Diagram showing delivery of GST-NRG1-ICD or GST proteins into GABAergic interneurons in *gtoGfp* slices. **l** Reduced Na^+ current density in GABAergic interneurons treated with GST-NRG1-ICD. Representative current traces of Na_v channels in GABAergic interneurons treated with recombinant GST or GST-NRG1-ICD proteins. Currents were elicited by step depolarizations from -80 to $+30$ mV in 5 mV increments from a holding potential of -80 mV. The tracts shown are for depolarizations from -80 to $+20$ mV. **m** I/V curves of Na_v channel activation in GABAergic interneurons treated with recombinant GST or GST-NRG1-ICD proteins. **Treatment $F(1, 24) = 10.89$, $P = 0.003$, two-way ANOVA, $n = 14$ cells treated with GST-NRG1-ICD, $n = 12$ cells treated with GST. Data are presented as mean values \pm SEM. **n** Similar voltage-dependent activation curves of Na_v channels in GABAergic interneurons treated with GST or GST-NRG1-ICD. Genotype $F(1, 24) = 0.059$, $P = 0.81$, two-way ANOVA, $n = 14$ cells treated with GST-NRG1-ICD, $n = 12$ cells treated with GST. Data are presented as mean values \pm SEM.

Next, we study whether NRG1-ICD plays a role in modulating Na_v currents in GABAergic interneurons. SCN1A contains four transmembrane domains (I–IV) and two major cytoplasmic loops (CL1 and CL2) (Fig. 5h). To investigate whether NRG1-ICD could interact with the CL of SCN1A, we purified GST-NRG1-ICD, His-CL1, and His-CL2 proteins from bacteria (Fig. 5i). As a negative control, GST proteins did not bind with the His-CL1 or His-CL2 (Fig. 5j). The CL1 and CL2 are important for the neuromodulation and membrane localization of SCN1A, respectively⁴¹. No interaction between NRG1-ICD and His-CL2 (Fig. 5j) implied that NRG1-ICD might not affect the membrane localization of SCN1A. In agreement, the protein levels of SCN1A in the membrane fraction were similar between control

and *gtoNrg1* mice (Supplementary Fig. 7c). However, NRG1-ICD could bind with His-CL1 (Fig. 5j), which suggested that NRG1-ICD might modulate the function of $\text{Na}_v1.1$ channel. To further test this hypothesis, we delivered 200 nM GST-NRG1-ICD or GST proteins (as a control) into GABAergic interneurons in *gtoGfp* slices through a recording pipette (Fig. 5k), and 10 min afterward recorded the Na_v currents using voltage clamp (Fig. 5l). The I/V curves of Na_v channel activation showed a downward shift in GABAergic interneurons treated with GST-NRG1-ICD, compared with control neurons (Fig. 5m). In accord, the maximal Na^+ current density was significantly reduced in GABAergic interneurons treated with GST-NRG1-ICD, compared with control neurons (GST-NRG1-ICD: -172.6 ± 11.61 pA/pF,

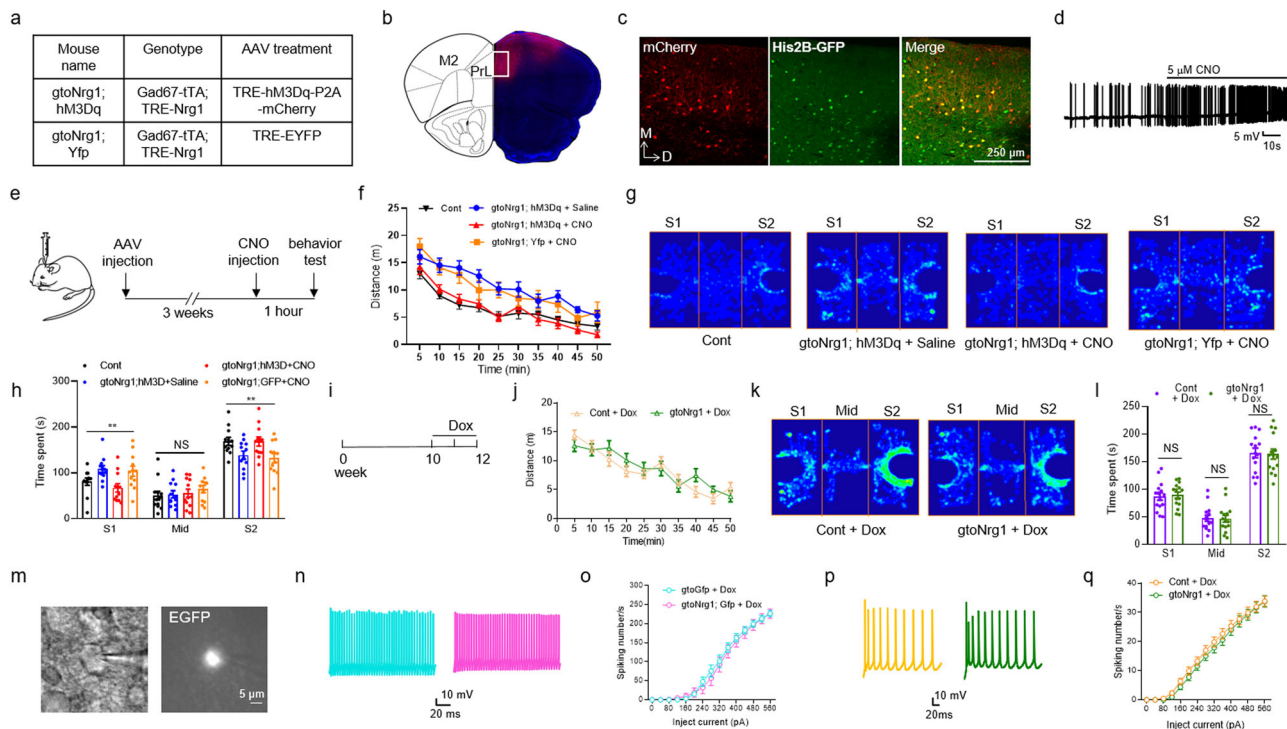


Fig. 6 Rescue of behavioral deficits and cortical disinhibition in *gtoNrg1* mice. **a** The genotype and AAV treatment in different mouse lines. **b** Diagram to show the brain regions infected by AAV. **c** Expression of mCherry in GABAergic interneurons from the rectangle in panel **b**. AAV expressing TRE-hM3Dq-P2A-mCherry were injected into the PFC of *gtoGfp* mice. The resulting PFC slices were subjected to immunofluorescence. Three independent experiments were repeated to get similar results. Scale bar, 250 μ m. **d** Increased firing of FS-GABAergic interneurons in the PFC slices of *gtoNrg1*; *Gfp* mice. The AP of FS-GABAergic interneurons were recorded before and after treatment with 5 μ M CNO. **e** Experimental design. Three weeks after stereotaxic injection of AAV, the mice were received i.p. injection of CNO (5 mg/kg) 1 h before behavioral tests. **f** Rescue of hyperactivity in *gtoNrg1*; hM3Dq mice by CNO. Shown is travel distance in the first 50 min during the open-field test. $F(3, 50) = 7.571$, $P = 0.0003$, two-way ANOVA, $n = 13$ for each group. Data are presented as mean values \pm SEM. **g** Occupancy plot of the heads from different groups of mice in the three-chamber test. S1, familiar mouse; S2, novel mouse. **h** Rescue of impaired social novelty in *gtoNrg1*; hM3Dq mice by CNO. Time spent in each chamber was quantified. NS not significant, $**P = 0.0068$ for S1, $**P = 0.0092$ for S2, one-way ANOVA, $n = 12$ for each group. Data are presented as mean values \pm SEM. **i** Experimental design. The 10-week-old control and *gtoNrg1* mice were treated with Dox for 2 weeks before the behavioral test. **j** Similar travel distance between Dox-treated control and *gtoNrg1* mice. Genotype $F(1, 24) = 0.0997$, $P = 0.7549$, two-way ANOVA, $n = 13$ for each group. Data are presented as mean values \pm SEM. **k** Occupancy plot of the heads from Dox-treated control and *gtoNrg1* mice in the three-chamber test. S1, familiar mouse; Mid, middle chamber; S2, novel mouse. **l** Similar social novelty between Dox-treated control and *gtoNrg1* mice. Time spent in each chamber was quantified. NS, not significant, two-sided t test, $n = 15$ for each group. Data are presented as mean values \pm SEM. **m** Expression of EGFP in the PFC slices from *gtoNrg1*; *Gfp* mice after treatment with Dox for 2 weeks. Four independent experiments were repeated to get similar results. Scale bar, 5 μ m. **n** Representative action potential traces of FS-GABAergic interneurons in Dox-treated *gtoGfp* and *gtoNrg1*; *Gfp* PFC. **o** Similar I/O curves of action potential from FS-GABAergic interneurons in Dox-treated *gtoGfp* and *gtoNrg1*; *Gfp* PFC. Genotype $F(1, 28) = 0.094$, $P = 0.762$, two-way ANOVA, $n = 15$ cells from four mice for each group. Data are presented as mean values \pm SEM. **p** Representative action potential traces of pyramidal neurons in Dox-treated *gtoGfp* and *gtoNrg1*; *Gfp* PFC. **q** Similar I/O curves of the action potential from pyramidal neurons in Dox-treated control and *gtoNrg1* PFC. Genotype $F(1, 57) = 0.433$, $P = 0.513$, two-way ANOVA, $n = 29$ cells from five *gtoGfp* mice, $n = 30$ cells from five *gtoNrg1*; *Gfp* mice. Data are presented as mean values \pm SEM.

$n = 14$, control: -225.3 ± 15.59 pA/pF, $n = 12$, $P = 0.0109$, t test). By contrast, membrane depolarizations required for half-maximal activation of Na_v channels were comparable between GABAergic interneurons treated with GST-NRG1-ICD and control neurons ($V_{1/2} = -29.86 \pm 0.76$ mV for GST-NRG1-ICD-treated neurons, $n = 14$, $V_{1/2} = -28.76 \pm 0.69$ mV for control neurons, $n = 12$, $P = 0.3023$, t test) (Fig. 5n). Together, these results indicated that acute application of NRG1-ICD into GABAergic interneurons attenuated the peak Na^+ current density but without changing the voltage dependence of Na_v channel activation, which is similar to the results in *gtoNrg1*; *Gfp* mice (Fig. 5c–e).

The causal link between cortical disinhibition and behavioral deficits. To further demonstrate whether cortical disinhibition in PFC causes behavioral deficits in *gtoNrg1* mice, we performed

rescue experiments using chemogenetic approaches. Toward this goal, we bilaterally injected adeno-associated virus (AAV) expressing TRE-hM3Dq-P2A-mCherry, an excitatory DREADD (designer receptors exclusively activated by designer drugs⁴²) or TRE-EYFP (as a control) into PFC of *gtoNrg1* mice. The resulting *gtoNrg1* mice expressing TRE-hM3Dq-P2A-mCherry or TRE-EYFP were named *gtoNrg1*; hM3Dq or *gtoNrg1*; Yfp mice, respectively (Fig. 6a). The brain regions infected by AAV were mainly PrL and M2 motor cortex (Fig. 6b). Since the expression of hM3Dq is controlled by TRE promoter and tTA, hM3Dq is only expressed in GABAergic interneurons from *gtoNrg1*; hM3Dq mice (Fig. 6c). Since we used the excitatory DREADD, administration of CNO increased the excitability of FS-GABAergic interneurons in *gtoNrg1*; hM3Dq mice (Fig. 6d).

Three weeks after AAV administration, mice were i.p. injected with CNO or saline 1 h prior to the behavioral test (Fig. 6e).

When *gtoNrg1*; hM3Dq mice were treated with saline, they showed hyperactivity compared with controls (Fig. 6f). However, they showed normal locomotion after treatment with CNO (Fig. 6f). The effects of CNO are specific because it cannot rescue hyperactivity in *gtoNrg1*; Yfp mice (Fig. 6f). These results indicate that activation of GABAergic interneurons in the PFC could rescue hyperactivity in *gtoNrg1* mice.

When *gtoNrg1*; hM3Dq mice were treated with saline, they showed impairment in social novelty compared with controls (Fig. 6g, h). However, the social novelty became normal in *gtoNrg1*; hM3Dq mice after treatment with CNO (Fig. 6g, h). The effects of CNO are specific because it cannot reverse impaired social novelty in *gtoNrg1*; Yfp mice (Fig. 6g, h). These results indicated that activation of GABAergic interneurons in the PFC could reverse the social behavioral deficit in *gtoNrg1* mice. Altogether, these data demonstrate a causal link between PFC disinhibition and behavioral deficits in *gtoNrg1* mice.

Dependence of behavioral deficits and cortical disinhibition on continuous NRG1 overexpression. Since *Gad67-tTA* starts to be expressed from embryonic stage²⁷, the phenotypes seen in *gtoNrg1* mice could be due to overexpressing NRG1 during development or the persistent NRG1 increase in adulthood. The rescue experiments using chemogenetic approaches suggested that the behavioral deficits in *gtoNrg1* mice might be reversible. To further test this hypothesis, adult mice at 2.5-month-old were fed with Dox-containing water for 2 weeks (Fig. 6i). To eliminate possible compounding effects of Dox, both control and *gtoNrg1* mice were subjected to Dox treatment. Notably, Dox-treated *gtoNrg1* and control mice traveled a similar distance in the open field (Fig. 6j), suggesting normal locomotive activity in Dox-treated *gtoNrg1* mice. In addition, Dox-treated *gtoNrg1* and control mice showed similar performance in the three-chamber test (Fig. 6k, l), indicating normal social novelty in Dox-treated *gtoNrg1* mice.

If the cortical disinhibition is a contributing mechanism, it should be diminished when NRG1 expression returned to normal levels. To test this notion, Dox-treated mice were subjected to electrophysiological recordings. Please note that EGFP is still visible in the *gtoNrg1*; Gfp PFC slices after treatment with Dox for 2 weeks (Fig. 6m) due to the long half-life of EGFP. These observations enable us to visualize GABAergic interneurons in the *gtoNrg1*; Gfp PFC slices after turning off NRG1 overexpression. The I/O curve of AP from FS-GABAergic interneurons was similar between Dox-treated *gtoGfp* and *gtoNrg1*; Gfp mice (Fig. 6n, o), indicative of normal excitability. Likewise, the enhanced firing rate of PN in *gtoNrg1* PFC also returned to control levels after Dox treatment (Fig. 6p, q). Altogether, these results demonstrate that behavioral deficits and cortical disinhibition in *gtoNrg1* mice require continuous NRG1 overexpression.

Discussion

In this study, we first analyzed *Nrg1* gene expression in the postmortem PFC and found increased type I *Nrg1* expression in GABAergic interneurons from schizophrenia patients, compared with age- and sex-matched controls. Then we generated *gtoNrg1* mice where type I *Nrg1* was specifically overexpressed in GABAergic interneurons. Intriguingly, *gtoNrg1* mice exhibited cortical disinhibition at the cellular, synaptic, and neural network levels. We further demonstrated that cortical disinhibition led to behavioral deficits. Lastly, we illustrated that both cortical disinhibition and behavioral deficits in *gtoNrg1* mice depended on continuous NRG1 overexpressing. In sum, our results demonstrate mechanisms underlying cortical disinhibition related to

schizophrenia and raise a possibility that relevant brain disorders may benefit from intervention to restore NRG1 signaling and GABAergic function.

Chemogenetic activation of GABAergic interneurons may increase tonic inhibition, but cannot restore the temporal organization of inhibitory transmission. Therefore, the rescue of locomotor and social novelty behavior by the chemogenetic manipulation suggests that these behaviors depend on tonic prefrontal inhibition, but do not require precise temporal regulation of this inhibition^{43,44}. In line with this notion, the schizophrenia-relevant behavioral deficit such as hyperactivity was also found in other pharmacological models of disinhibition in the forebrain regions^{45–48}.

Recent studies from single-cell RNA sequencing revealed that *Nrg1* is expressed in both glutamatergic and GABAergic neurons in mouse and human PFC^{16,17}. Previous studies mainly focused on the function of NRG1 in glutamatergic pyramidal neurons^{49–52}. Overexpression of *Nrg1* in pyramidal neurons led to glutamatergic hypofunction through inhibiting glutamate release or impairing NMDA receptor^{26,53–55}. This study showed that the excitability of FS-GABAergic interneurons was impaired in *gtoNrg1* mice where *Nrg1* was overexpressed in GABAergic interneurons. By contrast, the excitability of FS-GABAergic interneuron was not reduced in *ctoNrg1* mice where *Nrg1* was overexpressed in excitatory pyramidal neurons²⁶. Recent studies indicated that NRG1 was highly expressed in PV-positive GABAergic interneurons and was important for the plasticity of the visual cortex^{56,57}. Together, these results demonstrated the function of NRG1 in GABAergic interneurons.

gtoNrg1 mice exhibited an increased theta and delta oscillations in the PFC under freely behavioral conditions. By contrast, a previous study showed that overexpression of NRG1 in pyramidal neurons enhanced gamma oscillations in hippocampal slices⁵⁰. The discrepancy between these two studies might result from different neuronal types where NRG1 is overexpressed or the different conditions from in vivo and in vitro. Increased theta and delta oscillations are two of the consistent observations in schizophrenia patients⁵⁸. By contrast, both increased and reduced gamma oscillation have been reported in schizophrenia patients under different conditions⁵⁹.

The NRG1 EGF domain acts on the ErbB4 receptor which is mainly expressed in GABAergic interneuron^{35–37}. NRG1-ErbB4 signaling has been implicated in GABAergic circuitry formation^{35,60–63} and GABA transmission^{38–40,64,65}. However, ErbB4 was not activated in the PFC of *gtoNrg1* mice. The NRG1 protein levels in *gtoNrg1* PFC were 1.5–2-folds higher than controls and were much lower than other *Nrg1* transgenic mouse lines^{50,53}, which might explain why ErbB4 was not activated in *gtoNrg1* PFC. We further showed that the NRG1 EGF domain did not cause the reduction of Na_v currents in GABAergic interneurons. Indeed, the NRG1 EGF domain has been shown to increase the excitability of GABAergic interneurons through K^+ channels⁶⁶, albeit an opposite effect was observed in cultured hippocampal neurons⁶⁷.

On the other hand, NRG1-ICD can induce downstream signaling through protein–protein interaction and gene transcription^{7,26,68–70}. The reduced excitability of FS-GABAergic interneurons in *gtoNrg1* mice might be due to the effects of NRG1-ICD. In support of this hypothesis was the observation that NRG1-ICD could interact with the cytoplasmic loop 1 of SCN1A and inhibit the peak Na_v currents. The cytoplasmic loop 1 of SCN1A has been shown to interact with signaling proteins or be phosphorylated by protein kinases, which leads to the reduction of the peak Na_v currents^{41,71}. We speculate that the interaction of NRG1-ICD with the cytoplasmic loop 1 of SCN1A might account for the inhibition of peak Na_v currents by

NRG1-ICD. Given that NRG1-ICD but not NRG1 EGF domain attenuated peak I_{Na_v} currents in GABAergic interneurons, a parsimonious explanation of our finding is that the reduction of peak I_{Na_v} currents in *gtoNrg1* mice is due to NRG1-ICD. In sum, the data presented here demonstrate mechanisms underlying how *Nrg1* dysregulation impairs brain function, which might provide insight into the pathophysiological mechanisms of schizophrenia.

Methods

Generation of *gtoNrg1* mice. The TRE-*Nrg1* mice were generated as described in our paper²⁶. Briefly, *Nrg1*β1a was cloned into the EcoR V site of pMM400. An HA tag was inserted between Ig and EGF domains. A Not I fragment containing the transgene was used for transgenic mouse production. *Gad67-tTA* mice²⁷ were kindly provided by Dr. Yuchio Yanagawa, Gunma University, Japan. TRE-H2B-GFP reporter mice were from Jackson laboratory (005104). The TRE-*Nrg1* transgene mice and heterozygous *Gad67-tTA* knock-in mice were backcrossed with C57BL/6 mice for more than ten generations before cross-breeding. The resulting offspring contain four genotypes: wt, *Gad67-tTA*, TRE-*Nrg1*, and *gtoNrg1*. The *Gad67-tTA* heterozygous knock-in mice have an insertion of tTA cassette after the start codon of *Gad67* gene²⁷, which might disrupt *Gad67* gene expression. To avoid the potential knock-in effect on *Gad67* gene expression, we used *Gad67-tTA* mice as littermate controls for *gtoNrg1* mice. To eliminate the possible effects of the hormone cycle, male mice were used in all experiments. Animals were housed in rooms at 23 °C and 50% humidity in a 12 h light/dark cycle and with food and water available ad libitum. In some experiments, Dox (Sigma-Aldrich, catalog number D9891) was added to drinking water at 1 mg/ml in 2.5% sucrose. Animal experimental procedures were approved by the Institutional Animal Care and Use Committee of East China Normal University.

RT-qPCR and single-cell RT-PCR. The total RNA was isolated from the mouse brain and purified using Triazol (Invitrogen) and an RNAsasy mini kit (Qiagen), respectively. In total, 5 μg of total RNA was reverse transcribed using oligoT primers and SuperScript III reverse transcriptase (Invitrogen). One percent of the resulting cDNA was analyzed by qPCR in triplicates using SYBR Green/ROX (Fermentas) on Chromo 4 (Bio-Rad). The following primer pairs were used: type 1 *Nrg1*-F: gagtcagctcaggctccaagc; type 1 *Nrg1*-R: gtgatgtggca gaggcactgtc; *Gapdh*-F: gtggagctactctggaacatgtag; *Gapdh*-R: aatgttggaaggtcggtgtg. Levels of target mRNA levels were normalized to levels of *Gapdh* mRNA measured at the same time on the same reaction plate.

The PFC slices from *gtoNrg1*; *Gfp* mice were used for single-cell RT-PCR. The neurons expressing EGFP were GABAergic interneurons while the neurons with a triangle shape that do not express EGFP were excitatory pyramidal neurons. After a cell is patched, the intracellular contents are aspirated into the patch pipette and used for RT-PCR. Strict RNase-free solutions and pipettes were used for collecting single-cell RNA samples. We performed single neuron RT-PCR following the protocol in the paper⁷². The following primer pairs were used: HA-F: tgggaccagcatcgattaccat; HA-R: cgaccaccagcaggcgatag; vGat-F: tcacgacaaccaagatgac; vGat-R: gtcttctcttc tctgacag; vGlut1-F: cacagaagcccagttcaac; vGlut1-R: catgtttagggtggaggtag.

Immunofluorescence. The process of immunofluorescence analysis was performed as described by our previous studies²⁶. Briefly, brain slices were permeabilized with 0.3% Triton-X 100 and 5% BSA in PBS and incubated with primary antibodies at 4 °C overnight. After washing with PBS three times, samples were incubated with Alexa Fluor-555 secondary antibodies (goat-anti-mouse, A32727; goat-anti-rabbit, A32732; 1:1000, Thermo Fisher) for 1 h at room temperature. Samples were mounted with Vectashield mounting medium (Vector Labs) and images were taken by Leica TCS SP8 confocal microscope. The following primary antibodies were used: rabbit anti-NeuN (1:500, Abcam, ab177487), mouse anti-GABA (1:1000, Invitrogen, PA5-32241), and rabbit anti-neurogranin (1:1000, R&D, MAB7947). Unbiased stereology TissueFAX Plus ST (Tissue Gnostics, Vienna, Austria)⁷³ was applied to count EGFP-positive and NeuN-positive cell number in brain slices.

Western blot. Homogenates of PFC were prepared in RIPA buffer containing 50 mM Tris-HCl, pH 7.4, 150 mM NaCl, 2 mM EDTA, 1% sodium deoxycholate, 1% SDS, 1 mM PMSF, 50 mM sodium fluoride, 1 mM sodium vanadate, 1 mM DTT, and protease inhibitors cocktails. The supernatant of homogenate was subjected to centrifugation (25,000 × g × 1 h) to obtain the membrane fraction which was dissolved by RIPA buffer containing 1 M urea. All the protein samples were boiled in 100 °C water bath for 10 min before western blot. Homogenates or membrane protein were resolved on SDS/PAGE and transferred to nitrocellulose membranes, which were incubated in the TBS buffer containing 0.1% Tween-20 and 5% milk for 1 h at room temperature before the addition of primary antibody for incubation overnight at 4 °C. After wash, the membranes were incubated with HRP-conjugated secondary antibody (goat-anti-mouse, G-21040; goat-anti-rabbit, G-21234; 1:2000, Thermo Fisher) in the same TBS buffer for 1 h at room

temperature. Immunoreactive bands were visualized by ChemiDoc™ XRS + Imaging System (BIO-RAD) using enhanced chemiluminescence (Pierce) and analyzed with Image J (NIH). The following antibodies were used: rabbit anti-NRG1 (1:1000, Santa Cruz, sc-348), mouse anti-GAPDH (1:5000, Abways, ab0037), mouse anti-PSD95 (1:1000, Millipore, 2492127), rabbit anti-ErbB4 (1:1000, Cell Signaling, 111B2), rabbit anti-p-ErbB4 (1:200, Cell Signaling, Y1248) and rabbit anti- $I_{Na_v}1.1$ (1:500, Alomone Labs, ASC-001), mouse anti-GST (1:5000, ImmunoWay, B2101) and mouse anti-His (1:2000, ImmunoWay, B0401).

Behavior analysis. To eliminate possible effects that may be associated with the knock-in into *Gad67* gene, *Gad67-tTA* mice were used as controls in behavioral analysis. Behavioral tests were performed in 2.5–3-months old, male mice. The investigators for behavioral tests were blind to genotypes and/or Dox administration. Both control and *gtoNrg1* mice were treated with Dox to avoid possible compounding effects of Dox on behaviors. The behaviors were tested in the following order: open field, social interaction, social novelty, Y maze, and PPI. The intertest intervals are 2–3 days, except that between social interaction and novelty (30 min). The second batch of mice was used for nest building and buried food-finding test. The third batch of mice was used for behavioral tests after treatment with Dox. Mice were not tested for the same behavioral paradigms more than once, to avoid the effects of learning and memory.

Open field. Mice were placed in a chamber (27.9 × 27.9 × 20.3 cm) and monitored for movement for 50 min using an infrared camera placed above the box. The total distance, time in the center and margin of open field was measured by ANY-maze video tracking system (Stoelting).

Prepulse inhibition (PPI). PPI tests were conducted in the SR-LAB TM Startle Response System (San Diego Instruments). The motion of mice, placed in a Plexiglas tube mounted on a plastic frame, was monitored by a piezoelectric accelerometer. Before the test, mice were allowed to habituate to the chamber, to the 70-dB background white noise for 5 min, and to the prepulse (20 ms white noise at 75, 80, or 85 dB) and auditory-evoked startle stimuli (120 dB, 20 ms). In the PPI test, mice were subjected to 12 startle trials (120 dB, 20 ms) and 12 prepulse/startle trials (20 ms white noise at 75, 80, or 85 dB at 100-ms intervals and 20 ms 120-dB startle stimulus). Different trial types were presented pseudo-randomly with each trial type presented 12 times, and no two consecutive trials were identical. Mouse movement was measured for 100 ms after the startle stimulus onset (sampling frequency 1 kHz) for 100 ms. PPI (%) was calculated according to the formula: (100 – (startle amplitude on prepulse-pulse trials/startle amplitude on pulse alone trials) × 100).

Social interaction and novelty. Adult male mice were tested for social behavior in a three-chamber box (60 × 40 × 25 cm). Each of the end chambers contains a clear Plexiglas cylinder. One cylinder is the “social” cylinder, which contains a stimulus mouse (adult wild-type male mice who never met test mice). The other cylinder is “non-social” cylinder, which is empty. The test mice were first placed in the center chamber and allowed to freely explore the chambers with two empty cylinders for 10 min. For the social interaction test, mice were given an additional 5 min to explore the chambers with a “social” cylinder (S1) and a “non-social” cylinder (O). Thirty min after the social interaction test, the mice were subjected to a social novelty test. The test mice were given an additional 5 min to explore the chambers with cylinders containing a familiar mouse (S1) and a novel mouse (S2). Six-week-old male mice on a C57BL/6 background were used as social opponents. Sessions were video-recorded, and time spent around the “social” cylinder and “non-social” cylinder, or the familiar cylinder and novel cylinder were analyzed by the ANY-maze video tracking system (Stoelting). The box and cylinder were cleaned with 75% ethanol and dried thoroughly after each test session.

Y maze. The Y-maze apparatus was shaped like a Y and had three identical arms (25 × 10 × 10 cm) placed at an angle of 120° with respect to each other. The three arms were respectively labeled A (start arm), B (old arm), and C (new arm). There are different visual cues on the wall at the end of each arm. Mice were placed at the end of one arm (A) and allowed to freely navigate A and B arm for 5 min while C arm is blocked. Ten minutes later, C arm is opened, and the mice were allowed to freely explore all three arms for an additional 4 min. When the limbs of mouse were positioned in the arm was considered to have entered an arm. The activity of the mice was recorded and analyzed by the ANY-maze video tracking system (Stoelting). The apparatus was cleaned with 75% ethanol and dried thoroughly after each test session.

Nest building. One cotton square (5 × 5 cm) was placed in one cage with a single mouse. Twelve hours later, the nest was evaluated by a 5-point nest-rating scale⁷⁴. Each nest was evaluated by six independent investigators who are blinded to the genotype of the mice. The score of each nest was averaged by that from six investigators.

Buried food-finding test. The mice were subject to food deprivation 18 h before test. The test begins by placing a mouse in a clean cage (36 cm L × 20 cm W × 18 cm H)

containing 3 cm deep of clean bedding. The subject is allowed to acclimate to the cage for 5 min. Then the mouse was transferred to an empty clean cage. We buried 2 g food pellet ~1 cm beneath the surface, in a random corner of the cage. Smooth out the surface and reintroduce the mouse to the cage. The mouse is considered to have uncovered the food when it starts to eat, usually holding the food with forepaws. The latency to find the food was recorded by the investigator.

Recording in freely moving mice. The microdrive containing eight tetrodes (each tetrode has four channels) was prepared as described in our previous study⁷⁵. The mouse was anesthetized with pentobarbital sodium (40 mg/kg) before implanting the microdrive into PrL with the coordinates: anteroposterior (AP) 1.9 mm, mediolateral (ML) 0.5 mm relative to bregma. The tips of tetrodes were advanced to 1.4 mm from pia in the depth. After surgery, animals were housed in home cages to recover for 2 weeks. We used Plexon MAP system (Plexon, USA) to monitor neuronal signals. The tetrodes advanced 35 μ m every other day via rotating the screw. When the tetrodes reached layers 2–3 of PrL, the recording was started. The mouse behavior was monitored simultaneously by a video. The awake active state (speed >3 cm/s) was determined by the video and real-time spectrum. The power of LFP at a different frequency (delta: 1–3 Hz, theta: 4–12 Hz, alpha: 13–15 Hz, beta: 16–30 Hz, low gamma: 30–50 Hz, high gamma: 55–90 Hz, HFO: 100–300 Hz) was analyzed through Welch's averaged periodogram with a 1024-ms nonoverlapping Hanning window (NFFT = 2048) in combination with the function of PWELCH in Matlab R2013a.

Electrophysiology. TRE-*Nrg1* and *Gad67*-tTA mice showed no difference in electrophysiological studies, compared to wild-type mice. *Gad67*-tTA mice were used as controls in all electrophysiological studies. Mice were anesthetized by ketamine/xylazine (Sigma) and perfused transcardially for 1 min with 4 °C modified artificial cerebrospinal fluid (aCSF) containing (in mM) 250 glycerol, 2 KCl, 10 MgSO₄, 0.2 CaCl₂, 1.3 NaH₂PO₄, 26 NaHCO₃, and 10 glucose, to protect CNS neurons and maintain functional connectivity of brain slices. Mice were then decapitated and brains were quickly removed and chilled in ice-cold ACSF for an additional 1 min. Transverse mPFC slices (350 μ m) were prepared using a Vibroslice (VT 1000 S; Leica) in ice-cold ACSF. Slices were then incubated in regular ACSF containing (in mM): 126 NaCl, 3 KCl, 1.25 NaH₂PO₄, 1.0 MgSO₄, 2.0 CaCl₂, 26 NaHCO₃, and 10 glucose for 30 min at 34 °C for recovery, and then at room temperature (25 \pm 1 °C) for an additional 2–8 h. All solutions were saturated with 95% O₂/5% CO₂ (vol/vol). Dox (10 ng/ml) was present in the perfusate for experiments with slices from Dox-treated mice.

Whole-cell patch-clamp recordings from layers 2 to 3 PN in PrL were visualized with infrared optics using an upright microscope equipped with a \times 40 water-immersion lens (BX51WI; Olympus) and infrared-sensitive CCD camera. All data were obtained with a HEKA EPC10 double patch-clamp amplifier. Data were low-pass filtered at 10 kHz and digitally sampled at 10 kHz with PatchMaster version 2 \times 90.1. To record sEPSC and sIPSC, the pipettes were filled with the solution (in mM): 135 CsCH₃SO₃, 5 CsCl, 5 TEA-Cl, 20 HEPES, 0.4 EGTA, 2.5 Mg-ATP, 0.25 Na-GTP, and 1 QX314 (pH 7.25, 290 mOsm). Membrane potential was held at -70 mV for sEPSCs and 0 mV for sIPSCs, respectively. To record eIPSCs, the pipettes were filled with the solution (in mM): 130 CsCH₃SO₃, 10 CsCl, 10 HEPES, 0.2 EGTA, 1 MgCl₂, 4 Mg-ATP, 0.3 Na-GTP, and 5 QX314 (pH 7.25, 285 mOsm). The neurons were holding at -70 mV which were stimulated with a 100 μ s current injection by a nichrome-wire electrode placed 50–100 μ m from the soma of recorded neurons. To record mIPSCs, the concentration of CsCl was increased to 140 mM, CsCH₃SO₃ was omitted to enhance the driving force of Cl⁻, and 1 μ M TTX was added in the bath solution. To record Na_v currents, CdCl₂ (120 μ M) and CNQX (20 μ M) were added to the aCSF to block Ca²⁺ and AMPA receptor currents. The Na_v currents were evoked with a series of 100 ms depolarizations from a holding potential of -80 mV to $+30$ mV in 5 mV increments. Activation curves of Na_v channels were fitted to Boltzmann relationships. In all protocols, the intersweep interval was 2 s. Spontaneous and miniature events were analyzed using Mini Analysis Program (Synaptosoft). E/I ratio was calculated by (charge^{sEPSC} - charge^{sIPSC})/(charge^{sEPSC} + charge^{sIPSC}), where charge^{sEPSC} and charge^{sIPSC} represent total charge of sEPSC and sIPSC, respectively.

The action potential was recorded by the current-clamp. Neurons were held at -80 mV and were injected with different currents (duration, 500 ms; increments, \pm 20 pA; from -200 to 580 pA; interval, 10 s). The input–output relationship was defined as the number of action potentials versus the amplitude of current injection. Input resistance was determined as the slope of the linear regression of the I–V plot for a series of hyperpolarizing pulses, where I is current amplitude and V is the steady-state voltage. The basic electrophysiological characteristics were measured for the first action potential waveform during the depolarization. The action potential threshold was calculated as the voltage corresponding to the peak of the third differential of the action potential waveform. All data were performed with Neuroomatic version 3.0 (<http://www.neuromatic.thinkrandom.com>) which runs within Igor pro 6.7.3.2 (WaveMetrics).

GST pull-down. GST-tagged NRG1-ICD (amino acid 279 to 644 in rat NRG1 I β 1a proteins) were expressed in *Escherichia coli* BL21 cells and were purified using Glutathione SepharoseTM 4 Fast Flow (GE Health) according to the manufacturer's instructions. His-tagged cytoplasmic loop (CL) 1 and 2 of SCN1A were purified using Ni-NTA agarose beads (QIAGEN) following the manufacturer's protocols. For binding assays, eluted His-Na_v1.1-CL proteins were incubated with immobilized GST-NRG1-ICD or GST for 4 h at 4 °C. The mixture was then washed, eluted, and subjected to western blot with anti-His and anti-GST antibodies (Abmart).

Stereotaxic injection of AAV. For virus injection, *gtoNrg1* mice at age of 7–8 weeks were anesthetized with 1% pentobarbital sodium (100 mg/kg, i.p.) and were placed in a stereotaxic apparatus (RWD Life Science). Viruses were injected bilaterally in the PFC (PrL and M2 cortex) with the coordinates: anteroposterior (AP) 2.34 mm, mediolateral (ML) \pm 0.75 mm, dorsoventral (DV) -2.00 mm relative to bregma. Each injection used 0.5 μ l AAV and took 5 min. After injection, the glass pipette was left in place for 5 min in order to facilitate diffusion of the virus. The injection sites were examined at the end of the experiments, and animals with incorrect injection sites were excluded from the data analysis. Three weeks after AAV injection, mice were subjected to experiments. All surgery was conducted with an aseptic technique. The AAV expressing TRE-hm3Dq-P2A-mCherry or TRE-EYFP were generated in OBio Technology Corp., Ltd. The CNO is purchased from MCE company (HY-17366).

Statistical analysis. Two-way ANOVA was used in behavioral analysis including open field, PPI, and electrophysiological studies including I/O curve of AP, PPR, and I/V curves of Na_v channel activation. One-way ANOVA was used for the analysis of the data from three or more groups. Student's *t* test was used to compare data from two groups. Data were expressed as mean \pm SEM unless otherwise indicated. The sample size justification was based on the previous studies^{21,26,40}. According to the Wikipedia article on the normal distribution, about 95% of the values lie within two standard deviations. Our approach was to remove the data that were above (mean + 2*SD) and below (mean - 2*SD) before doing the statistical analysis. The example data shown were close to the overall mean. Statistically significant difference was indicated as follows: ****P* < 0.001, ***P* < 0.01, and **P* < 0.05. The statistical analysis was performed with the software of GraphPad Prism 8.

Reporting summary. Further information on research design is available in the Nature Research Reporting Summary linked to this article.

Data availability

All data supporting the results presented herein are available from the article paper, Supplementary Information, and Source Data. The full-length images for all the gels or blots are provided in Supplementary Fig. 10. The web-links of databases GSE93577 and GSE93987 are as follows: <https://www.ncbi.nlm.nih.gov/geo/query/acc.cgi?acc=GSE93577>, <https://www.ncbi.nlm.nih.gov/geo/query/acc.cgi?acc=GSE93987>. All unique materials used are readily available from the corresponding author upon request. Source data are provided with this paper.

Received: 8 September 2020; Accepted: 8 December 2020;

Published online: 12 January 2021

References

- Marin, O. Interneuron dysfunction in psychiatric disorders. *Nat. Rev. Neurosci.* **13**, 107–120 (2012).
- Stefansson, H. et al. Neuregulin 1 and susceptibility to schizophrenia. *Am. J. Hum. Genet.* **71**, 877–892 (2002).
- Stefansson, H. et al. Association of neuregulin 1 with schizophrenia confirmed in a Scottish population. *Am. J. Hum. Genet.* **72**, 83–87 (2003).
- Yang, J. Z. et al. Association study of neuregulin 1 gene with schizophrenia. *Mol. Psychiatry* **8**, 706–709 (2003).
- Mei, L. & Nave, K. A. Neuregulin-ERBB signaling in the nervous system and neuropsychiatric diseases. *Neuron* **83**, 27–49 (2014).
- Mei, L. & Xiong, W. C. Neuregulin 1 in neural development, synaptic plasticity and schizophrenia. *Nat. Rev. Neurosci.* **9**, 437–452 (2008).
- Wang, J. Y., Frenzel, K. E., Wen, D. & Falls, D. L. Transmembrane neuregulins interact with LIM kinase 1, a cytoplasmic protein kinase implicated in development of visuospatial cognition. *J. Biol. Chem.* **273**, 20525–20534 (1998).
- Bertram, I. et al. Immunohistochemical evidence for impaired neuregulin-1 signaling in the prefrontal cortex in schizophrenia and in unipolar depression. *Ann. N. Y. Acad. Sci.* **1096**, 147–156 (2007).

9. Parlapani, E. et al. Gene expression of neuregulin-1 isoforms in different brain regions of elderly schizophrenia patients. *World J. Biol. Psychiatry* **11**, 243–250 (2010).
10. Hashimoto, R. et al. Expression analysis of neuregulin-1 in the dorsolateral prefrontal cortex in schizophrenia. *Mol. Psychiatry* **9**, 299–307 (2004).
11. Law, A. J. et al. Neuregulin 1 transcripts are differentially expressed in schizophrenia and regulated by 5' SNPs associated with the disease. *Proc. Natl Acad. Sci. USA* **103**, 6747–6752 (2006).
12. Hahn, C. G. et al. Altered neuregulin 1-erbB4 signaling contributes to NMDA receptor hypofunction in schizophrenia. *Nat. Med.* **12**, 824–828 (2006).
13. Chong, V. Z. et al. Elevated neuregulin-1 and ErbB4 protein in the prefrontal cortex of schizophrenic patients. *Schizophr. Res.* **100**, 270–280 (2008).
14. Weickert, C. S., Tiwari, Y., Schofield, P. R., Mowry, B. J. & Fullerton, J. M. Schizophrenia-associated HapICE haplotype is associated with increased NRG1 type III expression and high nucleotide diversity. *Transl. Psychiatry* **2**, e104 (2012).
15. Liu, X. et al. Specific regulation of NRG1 isoform expression by neuronal activity. *J. Neurosci.* **31**, 8491–8501 (2011).
16. Saunders, A. et al. Molecular diversity and specializations among the cells of the adult mouse brain. *Cell* **174**, 1015–1030 e1016 (2018).
17. Zhong, S. et al. A single-cell RNA-seq survey of the developmental landscape of the human prefrontal cortex. *Nature* **555**, 524–528 (2018).
18. Lewis, D. A. & Sweet, R. A. Schizophrenia from a neural circuitry perspective: advancing toward rational pharmacological therapies. *J. Clin. Investig.* **119**, 706–716 (2009).
19. Birnbaum, R. & Weinberger, D. R. Genetic insights into the neurodevelopmental origins of schizophrenia. *Nat. Rev. Neurosci.* **18**, 727–740 (2017).
20. Mirnics, K. & Pevsner, J. Progress in the use of microarray technology to study the neurobiology of disease. *Nat. Neurosci.* **7**, 434–439 (2004).
21. Enwright Iii, J. F. et al. Transcriptome alterations of prefrontal cortical parvalbumin neurons in schizophrenia. *Mol. Psychiatry* **23**, 1606–1613 (2018).
22. Arion, D. et al. Distinctive transcriptome alterations of prefrontal pyramidal neurons in schizophrenia and schizoaffective disorder. *Mol. Psychiatry* **20**, 1397–1405 (2015).
23. Benzel, I. et al. Interactions among genes in the ErbB-Neuregulin signalling network are associated with increased susceptibility to schizophrenia. *Behav. Brain Funct.* **3**, 31 (2007).
24. Wang, Y. C. et al. Neuregulin 3 genetic variations and susceptibility to schizophrenia in a Chinese population. *Biol. Psychiatry* **64**, 1093–1096 (2008).
25. Chen, P. L. et al. Fine mapping on chromosome 10q22-q23 implicates Neuregulin 3 in schizophrenia. *Am. J. Hum. Genet.* **84**, 21–34 (2009).
26. Yin, D. M. et al. Reversal of behavioral deficits and synaptic dysfunction in mice overexpressing neuregulin 1. *Neuron* **78**, 644–657 (2013).
27. Tanaka, K. F. et al. Expanding the repertoire of optogenetically targeted cells with an enhanced gene expression system. *Cell Rep.* **2**, 397–406 (2012).
28. Geyer, M. A. & Braff, D. L. Startle habituation and sensorimotor gating in schizophrenia and related animal models. *Schizophr. Bull.* **13**, 643–668 (1987).
29. Corcoran, R., Mercer, G. & Frith, C. D. Schizophrenia, symptomatology and social inference: investigating “theory of mind” in people with schizophrenia. *Schizophr. Res.* **17**, 5–13 (1995).
30. Hoftman, G. D., Datta, D. & Lewis, D. A. Layer 3 excitatory and inhibitory circuitry in the prefrontal cortex: developmental trajectories and alterations in schizophrenia. *Biol. Psychiatry* **81**, 862–873 (2017).
31. Tumber, T. et al. Defining the epithelial stem cell niche in skin. *Science* **303**, 359–363 (2004).
32. Whittington, M. A., Faulkner, H. J., Doheny, H. C. & Traub, R. D. Neuronal fast oscillations as a target site for psychoactive drugs. *Pharm. Ther.* **86**, 171–190 (2000).
33. Yu, F. H. & Catterall, W. A. Overview of the voltage-gated sodium channel family. *Genome Biol.* **4**, 207 (2003).
34. Cheah, C. S. et al. Specific deletion of Nav1.1 sodium channels in inhibitory interneurons causes seizures and premature death in a mouse model of Dravet syndrome. *Proc. Natl Acad. Sci. USA* **109**, 14646–14651 (2012).
35. Fazzari, P. et al. Control of cortical GABA circuitry development by Nrg1 and ErbB4 signalling. *Nature* **464**, 1376–1380 (2010).
36. Vullhorst, D. et al. Selective expression of ErbB4 in interneurons, but not pyramidal cells, of the rodent hippocampus. *J. Neurosci.* **29**, 12255–12264 (2009).
37. Yau, H. J., Wang, H. F., Lai, C. & Liu, F. C. Neural development of the neuregulin receptor ErbB4 in the cerebral cortex and the hippocampus: preferential expression by interneurons tangentially migrating from the ganglionic eminences. *Cereb. Cortex* **13**, 252–264 (2003).
38. Woo, R. S. et al. Neuregulin-1 enhances depolarization-induced GABA release. *Neuron* **54**, 599–610 (2007).
39. Wen, L. et al. Neuregulin 1 regulates pyramidal neuron activity via ErbB4 in parvalbumin-positive interneurons. *Proc. Natl Acad. Sci. USA* **107**, 1211–1216 (2010).
40. Chen, Y. J. et al. ErbB4 in parvalbumin-positive interneurons is critical for neuregulin 1 regulation of long-term potentiation. *Proc. Natl Acad. Sci. USA* **107**, 21818–21823 (2010).
41. Catterall, W. A. From ionic currents to molecular mechanisms: the structure and function of voltage-gated sodium channels. *Neuron* **26**, 13–25 (2000).
42. Roth, B. L. DREADDs for Neuroscientists. *Neuron* **89**, 683–694 (2016).
43. Marissal, T. et al. Restoring wild-type-like CA1 network dynamics and behavior during adulthood in a mouse model of schizophrenia. *Nat. Neurosci.* **21**, 1412–1420 (2018).
44. Mukherjee, A., Carvalho, F., Eliez, S. & Caroni, P. Long-lasting rescue of network and cognitive dysfunction in a genetic schizophrenia model. *Cell* **178**, 1387–1402 e1314 (2019).
45. Bast, T., Zhang, W. N. & Feldon, J. Hyperactivity, decreased startle reactivity, and disrupted prepulse inhibition following disinhibition of the rat ventral hippocampus by the GABA(A) receptor antagonist picrotoxin. *Psychopharmacology* **156**, 225–233 (2001).
46. Enomoto, T., Tse, M. T. & Floresco, S. B. Reducing prefrontal gamma-aminobutyric acid activity induces cognitive, behavioral, and dopaminergic abnormalities that resemble schizophrenia. *Biol. Psychiatry* **69**, 432–441 (2011).
47. Israelashvili, M., Yael, D., Vinner, E., Belevsky, K. & Bar-Gad, I. Common neuronal mechanisms underlying tics and hyperactivity. *Cortex* **127**, 231–247 (2020).
48. Pezze, M., McGarrity, S., Mason, R., Fone, K. C. & Bast, T. Too little and too much: hypoactivation and disinhibition of medial prefrontal cortex cause attentional deficits. *J. Neurosci.* **34**, 7931–7946 (2014).
49. Agarwal, A. et al. Dysregulated expression of neuregulin-1 by cortical pyramidal neurons disrupts synaptic plasticity. *Cell Rep.* **8**, 1130–1145 (2014).
50. Deakin, I. H. et al. Transgenic overexpression of the type I isoform of neuregulin 1 affects working memory and hippocampal oscillations but not long-term potentiation. *Cereb. Cortex* **22**, 1520–1529 (2012).
51. Olaya, J. C. et al. Overexpression of neuregulin 1 type III confers hippocampal mRNA alterations and schizophrenia-like behaviors in mice. *Schizophr. Bull.* **44**, 865–875 (2018).
52. Deakin, I. H. et al. Altered hippocampal gene expression and structure in transgenic mice overexpressing neuregulin 1 (Nrg1) type I. *Transl. Psychiatry* **8**, 229 (2018).
53. Luo, X., He, W., Hu, X. & Yan, R. Reversible overexpression of bace1-cleaved neuregulin-1 N-terminal fragment induces schizophrenia-like phenotypes in mice. *Biol. Psychiatry* **76**, 120–127 (2014).
54. Papaleo, F. et al. Behavioral, neurophysiological, and synaptic impairment in a transgenic neuregulin1 (NRG1-IV) murine schizophrenia model. *J. Neurosci.* **36**, 4859–4875 (2016).
55. Kotzadimitriou, D. et al. Neuregulin 1 type I overexpression is associated with reduced NMDA receptor-mediated synaptic signaling in hippocampal interneurons expressing PV or CCK. *eNeuro* **5**, e0418-17.2018 1–18 (2018).
56. Sun, Y. et al. Neuregulin-1/ErbB4 signaling regulates visual cortical plasticity. *Neuron* **92**, 160–173 (2016).
57. Grieco, S. F. et al. Subanesthetic ketamine reactivates adult cortical plasticity to restore vision from amblyopia. *Curr. Biol.* **30**, 3591–3603 (2020).
58. Sponheim, S. R., Clementz, B. A., Iacono, W. G. & Beiser, M. Resting EEG in first-episode and chronic schizophrenia. *Psychophysiology* **31**, 37–43 (1994).
59. Lee, K. H., Williams, L. M., Breakspear, M. & Gordon, E. Synchronous gamma activity: a review and contribution to an integrative neuroscience model of schizophrenia. *Brain Res. Brain Res. Rev.* **41**, 57–78 (2003).
60. Flames, N. et al. Short- and long-range attraction of cortical GABAergic interneurons by neuregulin-1. *Neuron* **44**, 251–261 (2004).
61. Ting, A. K. et al. Neuregulin 1 promotes excitatory synapse development and function in GABAergic interneurons. *J. Neurosci.* **31**, 15–25 (2011).
62. Cahill, M. E. et al. Control of interneuron dendritic growth through NRG1/erbB4-mediated kalirin-7 disinhibition. *Mol. Psychiatry* **17**(1), 99–107 (2012).
63. Del Pino, I. et al. ErbB4 deletion from fast-spiking interneurons causes schizophrenia-like phenotypes. *Neuron* **79**, 1152–1168 (2013).
64. Tan, G. H. et al. Neuregulin 1 represses limbic epileptogenesis through ErbB4 in parvalbumin-expressing interneurons. *Nat. Neurosci.* **15**, 258–266 (2011).
65. Yin, D. M. et al. Calcyon stimulates neuregulin 1 maturation and signaling. *Mol. Psychiatry* **20**, 1251–1260 (2015).
66. Li, K. X. et al. Neuregulin 1 regulates excitability of fast-spiking neurons through Kv1.1 and acts in epilepsy. *Nat. Neurosci.* **15**, 267–273 (2011).
67. Janssen, M. J., Leiva-Salcedo, E. & Buonanno, A. Neuregulin directly decreases voltage-gated sodium current in hippocampal ErbB4-expressing interneurons. *J. Neurosci.* **32**, 13889–13895 (2012).
68. Bao, J., Wolpowitz, D., Role, L. W. & Talmage, D. A. Back signaling by the Nrg-1 intracellular domain. *J. Cell Biol.* **161**, 1133–1141 (2003).

69. Chen, Y., Hancock, M. L., Role, L. W. & Talmage, D. A. Intramembranous valine linked to schizophrenia is required for neuregulin 1 regulation of the morphological development of cortical neurons. *J. Neurosci.* **30**, 9199–9208 (2010).
70. Fazzari, P. et al. Cell autonomous regulation of hippocampal circuitry via Aph1b-gamma-secretase/neuregulin 1 signalling. *eLife* **3**, e02196 (2014).
71. Smith, R. D. & Goldin, A. L. Phosphorylation of brain sodium channels in the I–II linker modulates channel function in *Xenopus* oocytes. *J. Neurosci.* **16**, 1965–1974 (1996).
72. Citri, A., Pang, Z. P., Sudhof, T. C., Wernig, M. & Malenka, R. C. Comprehensive qPCR profiling of gene expression in single neuronal cells. *Nat. Protoc.* **7**, 118–127 (2011).
73. Yu, Q. et al. Genetic labeling reveals temporal and spatial expression pattern of D2 dopamine receptor in rat forebrain. *Brain Struct. Funct.* **224**, 1035–1049 (2019).
74. Deacon, R. M. Assessing nest building in mice. *Nat. Protoc.* **1**, 1117–1119 (2006).
75. Lin, L. et al. Large-scale neural ensemble recording in the brains of freely behaving mice. *J. Neurosci. Methods* **155**, 28–38 (2006).

Acknowledgements

This work was supported by grants from National Natural Science Foundation of China (No. 81471118 and 31861143033); grants from Shanghai Key Laboratory of Psychotic Disorders (No. 13dz2260500); grants from State Key Laboratory of Neuroscience. Dr. Dong-Min Yin is a NARSAD Young Investigator. We thank Dr. Yuchio Yanagawa for proving *Gad67-tTA* mice.

Author contributions

Y.-Y.W. performed biochemical and behavioral experiments. B.Z. performed the electrophysiology recordings in brain slices. M.-M.W. and L.L. performed in vivo recordings. X.-L.Z. assisted the biochemical experiments. Y.-Y.W., B.Z., L.L., and D.-M.Y. analyzed the data. D.-M.Y. designed the experiments, supervised the work, and wrote the paper.

Competing interests

The authors declare no competing interests.

Additional information

Supplementary information is available for this paper at <https://doi.org/10.1038/s41467-020-20552-y>.

Correspondence and requests for materials should be addressed to D.-M.Y.

Peer review information *Nature Communications* thanks Tim Karl and other, anonymous, reviewers for their contributions to the peer review of this work. Peer review reports are available.

Reprints and permission information is available at <http://www.nature.com/reprints>

Publisher's note Springer Nature remains neutral with regard to jurisdictional claims in published maps and institutional affiliations.



Open Access This article is licensed under a Creative Commons Attribution 4.0 International License, which permits use, sharing, adaptation, distribution and reproduction in any medium or format, as long as you give appropriate credit to the original author(s) and the source, provide a link to the Creative Commons license, and indicate if changes were made. The images or other third party material in this article are included in the article's Creative Commons license, unless indicated otherwise in a credit line to the material. If material is not included in the article's Creative Commons license and your intended use is not permitted by statutory regulation or exceeds the permitted use, you will need to obtain permission directly from the copyright holder. To view a copy of this license, visit <http://creativecommons.org/licenses/by/4.0/>.

© The Author(s) 2021